Nanoscale

ROYAL SOCIETY OF CHEMISTRY

PAPER

View Article Online
View Journal | View Issue

Cite this: *Nanoscale*, 2021, **13**, 7348

A rapid and sensitive fluorescence biosensor based on plasmonic PCR†

Jingrui Wu,‡[a] Kunlun Jiang, ‡[a] Hua Mi,[a] Yuwei Qiu,[a] Jiwoong Son,[b] Hyun June Park,[c] Jwa-Min Nam [b] and Jung-Hoon Lee *[a]

Received 7th January 2021,
Accepted 16th March 2021

DOI: 10.1039/d1nr00102g

rsc.li/nanoscale

Plasmonic PCR utilizing metallic nanoparticles has shown great advantages compared to the commercial thermocycler equipment in terms of cost, size and processing time. However, due to the strong fluorescence quenching, plasmonic nanoparticle-based PCR requires additional post-processing steps such as centrifugation and gel electrophoresis. This process increases the overall diagnostic time, offsetting the benefits of fast thermocycling. Here, we report a rapid and sensitive plasmonic photothermal PCR (PPT-PCR) assay method based on *in situ* end-point fluorescence detection. By using plasmonic magnetic bi-functional nanoparticles, PPT-PCR involving 30 thermocycles and fluorescence detection following magnetic separation has successfully shown that DNA targets can be detected within 5.5 minutes. The limit of detection (3.3 copies per μL) is comparable with that of the conventional real-time quantitative PCR; however, the assay time is about 5.5 times shorter for the PPT-PCR. The strategy of combining the photothermal effect and magnetic separation into a single particle will open new horizons in the development of fast and sensitive PCR-based biosensors for point-of care testing.

Introduction

Nucleic acid amplifications (NAAs) represent important and valuable tools for chemists, biologists, and medical scientists and have found extensive use in most fields of biological and medical research.[1–3] With the 2019 pandemic of coronavirus (COVID-19), there is an increasing need for fast and reliable NAA tools to find the cause of infection and contain it.[4–10] In particular, due to its ability to detect trace amounts of nucleic acids,[11–13] diagnosis based on polymerase chain reaction (PCR) has been considered as a standard method for identifying many diseases.[14–21] Real-time quantitative PCR (qPCR) is the most widely used tool for diagnostic testing because of its fast analysis time and because there is no need for post-processing.[15,22] However, disadvantages such as heavy and time-consuming instruments (~1 to 2 hours) and high price (~20 K USD) make it difficult to apply conventional PCR to point-of-care diagnosis (POC).[23,24]

Recently, PCR systems using plasmonic metallic nanoparticles have become an active research area and shown advantages in terms of time and cost.[25,26] Nonradiative relaxation of absorbed light by nanoparticles can be converted to significant thermal energy through photoexcitation of plasmons or through electron–phonon and phonon–phonon coupling, resulting in rapid and localized heat around nanostructures.[27–31] Utilizing light-to-heat conversion, known as the plasmonic photothermal effect, can reduce the overall thermocycling time, the core process of PCR, to less than 10 minutes.[25,26,31–36] However, many of these methods still require post-processing and complex sample preparation and replacement protocols, making them less attractive for widespread use. In addition, the strong light absorption of these nanoparticles can significantly attenuate the fluorescent signals emitted by widely used fluorescent reporters, which limits the ability to quantify amplification products in nanoparticle-based PCR systems.[28,35] Recently, plasmonic photothermal PCR using anisotropic gold nanoparticles has shown that real-time quantitative analysis is possible by preventing photobleaching using an infrared (IR) light source and increasing the signal-to-noise ratio using a large amount of fluorescent reporters.[31] However, the large amount of fluorescent reporters can inhibit PCR and cause non-specific amplification which would interfere with quantification.[37]

Here, we report a fast, sensitive and quantitative plasmonic photothermal (PPT)-PCR method based on end-point fluorescence detection using plasmonic magnetic nanoparticles

[a]*Department of Chemistry, City University of Hong Kong, Hong Kong SAR, China. E-mail: junghlee@cityu.edu.hk*
[b]*Department of Chemistry, Seoul National University, Seoul 08826, South Korea*
[c]*Department of Biotechnology, Duksung Women's University, Seoul, South Korea*

†Electronic supplementary information (ESI) available: HRTEM, XRD&FFT patterns, device setup, optimization condition of thermocycling, photothermal conversion efficiency calculation, and results from conventional PCR. See DOI: 10.1039/d1nr00102g

‡These authors contributed equally.

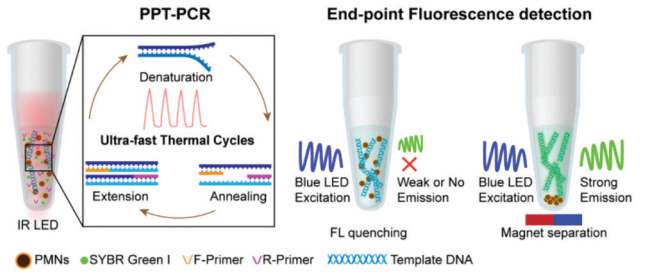

Fig. 1 Schematic illustrations of the plasmonic photothermal (PPT)-PCR method based on *in situ* end-point fluorescence detection using plasmonic magnetic nanoparticles (PMNs).

(PMNs) for molecular diagnostics (Fig. 1). Rapid DNA amplification and quantitative detection were achieved using specially designed core–shell bi-functional nanoparticles. Gold shells were used as nano-sized heaters to achieve ultrafast PCR thermocycling based on the plasmonic photothermal effect. By irradiating light with a resonance wavelength to the Au shell, the heat converted from light by nanoparticles can be quickly and uniformly transferred to the surroundings, and the temperature of the PCR for DNA amplification can be controlled by periodically adjusting the LED operating power. To enhance the saturation magnetization, a superparamagnetic nanocluster core composed of small-sized iron oxide nanoparticles was synthesized and used for ultrafast magnetic separation for *in situ* fluorescence signal detection. Fast separation of PMNs using an external magnetic field can reduce the fluorescence quenching of SYBR green I (SG), which is commonly used in quantitative PCR protocols. We showed that PPT-PCR integrated with fast end-point fluorescence detection can be used for fast, sensitive and quantitative biomarker detection. We achieved 30 thermocycles between 72 °C and 95 °C in <4.2 minutes with a 10 μL reaction volume, corresponding to a heating ramp rate of 8.71 ± 0.36 °C s^{-1} and a cooling ramp rate of 5.51 ± 0.22 °C s^{-1}. The calculated limit of detection (LOD, 3.3 copies per μL) was similar to that of conventional real-time PCR equipment, but the analysis time was reduced by about 5.5 times for PPT-PCR.

Experimental

Chemicals and instruments

All chemicals were of analytical grade and used as received without further purification. Iron(III) chloride hexahydrate ($FeCl_3{\cdot}6H_2O$), ethylene glycol (EG), sodium acetate (NaOAc), sodium citrate (Na_3Cit), tetrachloroauric acid trihydrate ($HAuCl_4{\cdot}3H_2O$), (3-aminopropyl) trimethoxysilane (APTMS), tetrakis(hydroxymethyl)phosphonium chloride solution (THPC), sodium hydroxide (NaOH), and potassium carbonate (K_2CO_3) were purchased from Sigma Aldrich. Formaldehyde (FA) was purchased from TCI. mPEG-thiol (M.W. = 5k) was purchased from Laysan Bio, Inc. KAPA2G Fast PCR Kit was purchased from Roche. HPLC purified forward primer (5′-ATC AAA CGG CAG GCA GAA CAG G-3′) and reverse primer (5′-ACA GGG ACA TCG CCA CCA GAA A-3′), dNTP mix, nuclease free water, SYBR safe and SYBR Green I (SG) were purchased from Thermo Fisher Scientific. Quick-Load® purple low molecular weight DNA ladder, Quick-Load purple 1 kb DNA ladder and gel loading dyes were purchased from New England BioLabs, Inc. Mineral oil and transparent PCR tube and cap were purchased from Bio-Rad Laboratories. Optical spectra were monitored by using a UV-vis-IR spectrometer (Cary 60, Agilent). Morphology and size distribution of PMNs and other intermediates were examined with a transmission electron microscope (TEM, Tecnai 12, Philips) and field emission TEM (FE-TEM, JEM-F200, JEOL).

Preparation of magnetic nanoclusters

Iron oxide magnetic nanoclusters were synthesized by a reported method with modifications.[38] Typically, $FeCl_3{\cdot}6H_2O$ (0.68 g, 2.5 mmol), sodium acetate (1.2 g, 0.015 mol), Na_3Cit (0.22 g, 0.75 mmol) and 400 μL deionized water (DIW) were added in 20 mL ethylene glycol. After 2 h of sonication at 30 °C, a dark yellow solution formed, which was transferred to a Teflon-lined stainless-steel autoclave reactor. The solution was maintained at 200 °C for 12 h and then naturally cooled down to room temperature. The mixture was then washed with 20 mL ethanol (EtOH) and 20 mL DIW 2 times each, followed by 24 h of drying at 60 °C. Five milligrams of as-prepared magnetic nanocluster powder was dispersed in 10 mL EtOH, and 500 μL of APTMS was then added to the solution. After being vortexed for 12 h at 1000 rpm, the particles were collected by using a magnet and washed with 10 mL DIW 3 times.

Preparation of plasmonic magnetic nanoparticles (PMNs)

Au seed colloids were prepared using a reported method.[39] Briefly, 6640 μL of 1 M NaOH solution was mixed with 600 mL of DIW followed by the addition of 160 μL of the reducing agent THPC. Finally, 24 mL of 1% (wt/wt) $HAuCl_4{\cdot}3H_2O$ was added to the vials under constant stirring. After being stirred for 30 seconds, the solution was moved to a refrigerator and stored at 4 °C. The solution was 5 times concentrated before use. Ten microliters of as-prepared magnetic nanocluster–NH_2 was mixed with 10 mL of 5 times concentrated Au colloid solution, followed by the addition of 1.5 mL of 1 M NaCl. The mixture was vortexed at 1000 rpm for 12 h. Magnetic nanocluster–Au seed particles were washed with 20 mL of DIW three times, and redispersed in 2.5 mL of DIW. For the formation of the Au shell, a plating solution was prepared.[39] Typically, 500 mL of 1.8 mM K_2CO_3 was mixed with 10 mL of 1% (wt/wt) $HAuCl_4{\cdot}6H_2O$. The mixture was stirred at 400 rpm overnight. After that, 1 mL of magnetic nanocluster–Au seed nanoparticles was added to 200 mL of the plating solution at 600 rpm after 1 min of sonication; then 400 μL of 37% FA was quickly added to the reaction solution. After the formation of the Au shell (30 min), 2 mL of 1% Tween-20 in DIW was added to the reaction solution. After 2 h of stirring, the mixture was centrifuged (1500 RCF, 10 min) and washed with 40 mL of DIW three times. Finally, PMNs were redispersed in 8 mL

DIW. Eight milliliters of PMNs in DIW was added to 8 mL of 1% mPEG–thiol solution and vortexed at 1000 rpm overnight. The reaction mixture was centrifuged (1500 RCF, 10 min) and washed with 40 mL of DIW 3 times. Finally, PMNs were redispersed in 1 mL of 1% BSA and kept at 4 °C for 24 h.

PPT-PCR optical device

Infrared-LED (850 nm peak wavelength, mounted on a metal core PCB, 8.5 W power rating, 3.8 W radiant flux (at 700 mA forward current, 12.4 V forward voltage), LZ4-40R608, LED Engine, CA, USA) was used for the plasmonic heating of PMNs, controlled by a power supply (Keithley-2230G-30-1 triple channel DC power supply, Tektronix, Inc., OR, USA). A 20.0 mm focus spot top lens fiber coupling (10 356, Carclo Optics, PA, USA) was used to focus the light on the samples. Blue-LED (5 mm, 480 nm peak wavelength, 3.2 V forward voltage, 20 mA forward current, 4.1 cd, C503B-BCN-CV0Z0461, CREE, Inc., NC, USA), FITC excitation filter (center wavelength = 475 nm, bandwidth = 35 nm, MF475-35, Thorlabs, Inc., NJ, USA) were used for the excitation of SYBR® Green I, and a spectrophotometer (CCS200, Thorlabs, Inc., NJ, USA) and optical fibers (M0065-51-0034, Thorlabs, Inc., NJ, USA) were used for the collection of fluorescent emission signals for *in situ* end-point measurements. The temperature was measured and recorded with an IR thermometer (OPTCSTCLT15, Optcs, GER) and thermal camera (FLK-100-CLKT, Fluke, WA, USA). Thermocycling with LED, power supply, fluorescence measurement, cooling fans, and temperature measurement were controlled with the LabVIEW program.

Preparation of PCR

Two microliters of 5x PCR buffer, 0.5 μL 10 μM F-Primer, 0.5 μL 10 μM R-Primer, 0.2 μL 10 mM dNTP, 0.04 μL 5 U μL^{-1} KAPA2G Fast polymerase, 0.5 μL 20x SYBR Green I in DMSO, and 0.26 μL nuclease free water was mixed as a master mix solution. For PPT-PCR, PMNs in 1% BSA was centrifuged and re-dispersed in 0.4% BSA of the same volume. In a 10 μL reaction, 5 μL PMNs in 0.4% BSA was mixed with 4 μL master mix solution. After adding 1 μL Lambda DNA template solution, 20 μL mineral oil was added to avoid the evaporation of water during thermocycling. For PCR by a conventional thermocycler, 5 μL nuclease free water and 1 μL Lambda DNA template solution were mixed with 4 μL master mix solution. PCR products were analyzed by mixing 3 μL of 6× loading buffer and 5 μL of DIW with 10 μL reaction solution and loading 5 μL of the mixture on 3% agarose gels with SYBR safe staining. A DNA ladder was used to confirm the size of products.

Results and discussion

Plasmonic magnetic nano-sized heaters

Rapid plasmonic PCR and end-point fluorescence detection are based on light-driven photothermal heating and the magnetic properties of bi-functional PMNs. As the optical properties of core–shell nanoparticles highly depend on the size

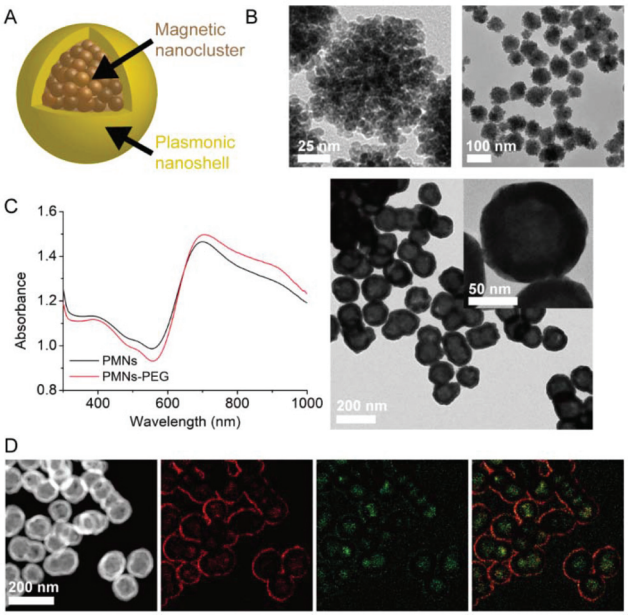

Fig. 2 (A) Scheme of PMNs. (B) TEM images of the magnetic nanocluster core. (C) UV-vis-IR spectrum and TEM image of PMNs. (D) High-angle annular dark-field image (HAADF) and elemental mapping images of PMNs, where Au and Fe elements are displayed as red and green colors.

of the core and shell, we synthesized particles composed of an 80 nm magnetic nanocluster core and a 20 nm gold shell to use the IR light source (Fig. 2A). Iron oxide magnetic nanoclusters were prepared by modified solvothermal synthesis (81.8 nm ± 5.6 nm) (Fig. 2B and S1A†).[38] The nanoclusters are composed of small-sized iron oxide nanoparticles (5 to 10 nm) and exhibit the collective behavior of individual nanoparticles, increasing the magnetic moment while maintaining superparamagnetic behaviour (Fig. S1D–F†). After being functionalized with amino groups, magnetic nanoclusters were further coated with an ~2 nm Au colloid (Fig. S1B†), followed by seed-mediated growth of the Au shell (Fig. 2C and S1C†).[39,40] The average diameter of PMNs was confirmed as 122.2 nm ± 6.9 nm. Next, surface modifications of PMNs with mPEG–thiol were employed to minimize the nonspecific interaction between PMNs and PCR reagents. UV-vis spectra and TEM were used to characterize the optical properties and morphology of PMNs (Fig. 2C). The UV-vis spectrum shows that PMNs have strong light absorption properties in the IR wavelength region, indicating that they are suitable for photothermal conversion by nanoparticles with 850 nm IR light irradiation.[41] The crystalline structure of iron oxide nanoclusters and PMNs was analyzed with high-resolution TEM and X-ray diffractometer (Fig. S1 and S2†). The differences on the XRD patterns between iron oxide nanoclusters and PMNs are matched with the results from HAADF and EDS elements mapping. The results indicate that the magnetic core is completely encapsulated by the Au shell (Fig. 2D). Therefore, PMNs are ideal for fluorescence-based analysis as they can avoid

photobleaching of fluorescent dyes (SYBR Green I, excitation = 497 nm and emission = 520 nm) caused by prolonged light exposure.

Plasmonic thermocycling for nucleic acid amplifications

By using specially designed plasmonic magnetic bi-functional nanoparticles, the photothermal properties are systematically investigated. In the designed particles, the magnetic core provides the magnetic properties that can be used to quickly separate particles using magnets, enabling rapid fluorescence detection, and the Au shell generates heat due to its photothermal properties when irradiated with IR light. For fast photothermal conversion, a home-built photothermal device with an 850 nm IR-LED light for heating, a fan for cooling (operates only during the cooling process), and an IR temperature sensor that accurately measures and records the temperature of the solution were used (Fig. S3†). Compared to thermocouples that require contact detection of a solution, non-contact temperature measurement can prevent contamination of samples and reduce the time required to prepare an experiment.[31] Because the photothermal conversion efficiency is directly correlated to the strength of the absorption property of the nanoparticles, we first demonstrated thermocycling using PMNs with different concentrations (Fig. 3). Representative temperature profiles were obtained from rapid thermocycling (30 cycles) between 72 °C and 95 °C with a fixed solution volume of 10 μl and varying optical density (OD) of PMNs (Fig. S4†). Fig. 3A shows the heating and cooling ramp rates (extracted from Fig. 3B) calculated by dividing the temperature difference between 72 °C to 95 °C with the measured time interval between the two temperatures. The absorption of photons by gold nanoparticles has no significant way to lose energy other than the release of heat to the surroundings.[36,42] Therefore, a linear increase in heating ramp rate is expected with the increase in nanoparticle concentration, which is in good agreement with our experimental results (Fig. 3A). The results showed a decrease in the time necessary to achieve 30 cycles when the OD of the PMNs was increased from 2.0 to 14.0.

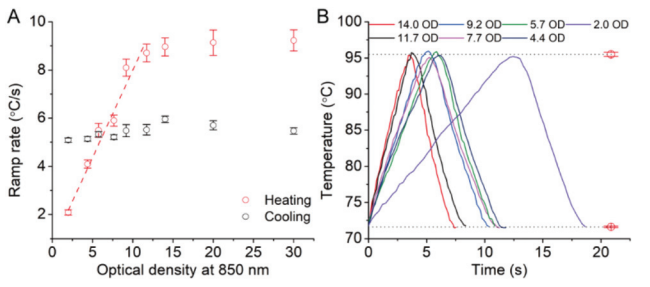

Fig. 3 (A) Heating and cooling ramp rates of samples with different concentrations of PMNs. The dashed line shows the linear regression of the heating ramp rate: rate = 0.731994 + 0.726563OD (R^2 = 0.97861). (B) Temperature profile of one thermocycle with different concentrations of PMNs.

The shortest thermocycling time for 30 cycles was confirmed to be 253 ± 5.3 seconds for the 14.0 OD sample (10 μL solution), which corresponds to the heating and cooling ramp rates of 8.71 ± 0.36 °C s^{-1} and 5.51 ± 0.22 °C s^{-1}, respectively (Fig. 3A and S3†). The heating and cooling ramp rates can be further increased by reducing the reaction volume (Fig. S7†). The accuracy of the set temperature was 95.5 ± 0.27 °C and 71.6 ± 0.11 °C for 95 and 72 °C. There was no significant improvement of the heating rates when the OD was increased above 14.0 (Fig. 3A). This can be caused by a reduced light penetration depth or plasmonic coupling between close particles as the concentration of nanoparticles increases.[36,43,44] No significant heating was observed without PMNs in the IR-LED irradiation (Fig. S5†). The changes in the UV-vis-IR spectrum were monitored to confirm the thermal stability of PMNs, and no spectral changes were detected after 30 photothermal cycles from 72 °C to 95 °C (Fig. S6†). Furthermore, we also optimized the heating rate with different sample volumes and different working currents of IR-LED (Fig. S7†). Unless otherwise specified, 14.0 OD of PMNs and 10 μL of solution volume were used for all experiments.

Validation of PPT-PCR amplification and fluorescence-based detection

After obtaining the optimal ramp rate determined by LED intensity and particle concentration studies, the system was applied to evaluate the analytical performance of PPT-PCR for trace nucleic acid amplification and fluorescence-based detection. As shown in Fig. 4, PPT-PCR was conducted in two steps: 30 thermocycles between 95 °C (0 seconds, denaturation) and 72 °C (2 seconds, annealing/extension) including an initial denaturation of 20 seconds at 95 °C. Volumetric uniform

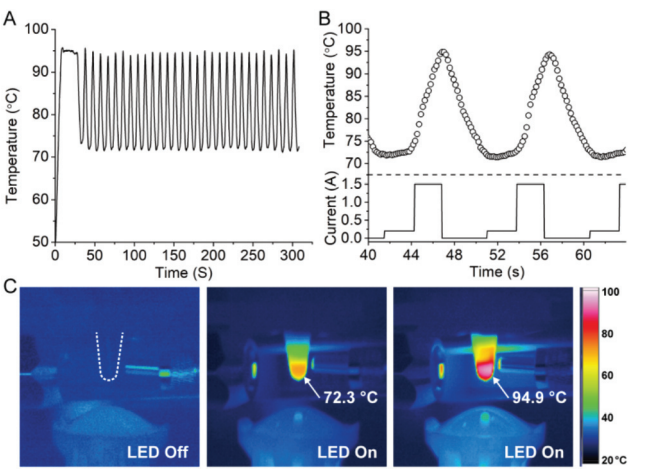

Fig. 4 (A) PPT-PCR temperature profile of the two steps for the 30 thermocycles between 95 °C (0 seconds, denaturation) and 72 °C (2 seconds, annealing/extension) including an initial denaturation of 20 seconds at 95 °C. (B) Temperature execution profile performed by the photothermal LED device. (C) Thermographic camera images of PMN solution upon IR-LED irradiation.

heating by PMNs were further confirmed by using a thermographic camera. The images showed that the solution temperature changed rapidly from room temperature to 72 °C and 95 °C only when irradiated with IR-LED light (Fig. 4C). To demonstrate PPT-PCR, Lambda DNA was amplified with the PMNs (14.0 OD) and SG (1×) by using our homebuilt LED-device. The temperature profile shows that the two steps of 30 thermocycles including initial denaturation can be completed in ~300 seconds (Fig. 4A). Since the emission of fluorescent dyes close to the nanoparticle surface in colloidal suspensions undergoes significant quenching,[45] the PMNs need to be removed from the reaction solutions to measure the clear and strong fluorescence signal from the amplicons. After the PPT-PCR amplification reactions, we applied an external magnetic field to collect the PMNs to the bottom of the PCR tube for *in situ* fluorescence detection. The amplification reaction was confirmed by measuring the fluorescence signal produced by SG upon excitation from a blue LED. Fig. 5 shows the fluorescence image and scheme of sample before and after magnetic separation. Without magnetic separation, no detectable fluorescence emission was measured due to fluorescence quenching and spectral overlap with PMNs (Fig. 5A). In comparing with the smaple in Fig. 5A, the stronger fluorescence intensity of the sample in Fig. 5B indicate that magnetic separation can contribute to rapid fluorescence detection is indispensable for reliable measurements. Besides, the PCR efficiency and quenching effect in relation to PMN concentration were studied (Fig. S8†).

PPT-PCR quantification *via in situ* end-point fluorescence measurement

To evaluate the analytical LOD of PPT-PCR, a serial dilution of Lambda DNA templates was prepared and amplified by PPT-PCR. Forward and reverse primers were designed to amplify 100-nucleotides from the Lambda DNA sequence. Fig. S9† shows a characteristic fluorescence spectrum of DNA-SG. The fluorescence intensity of amplicon at 525 nm was measured after the magnetic separation and plotted against template DNA concentrations for quantification

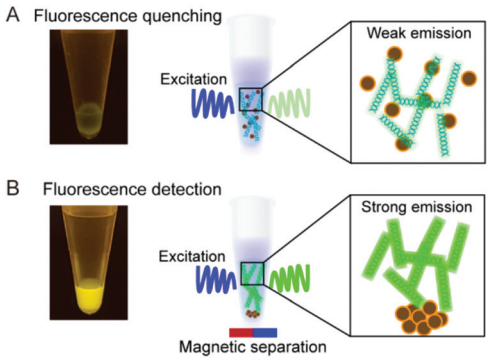

Fig. 5 Fluorescence image and scheme of reaction solution before (A) and after (B) magnetic separation of PMNs.

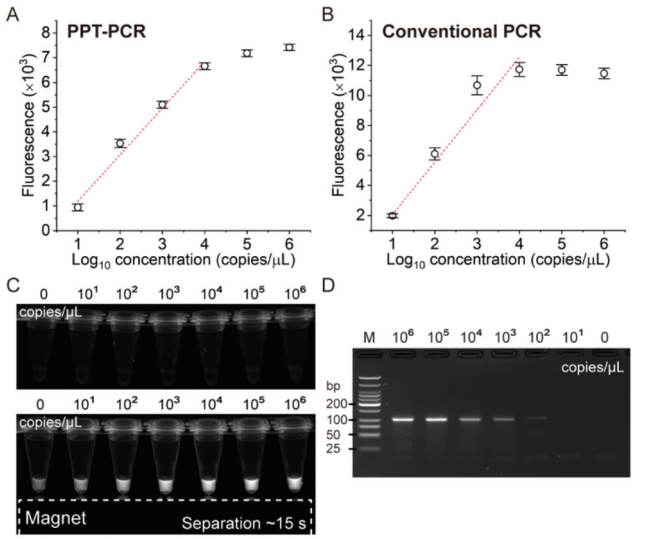

Fig. 6 (A) End-point fluorescence intensity plot of PPT-PCR against Lambda DNA template concentration (integration time: 200 milliseconds). (B) End-point fluorescence intensity plot of the conventional PCR. (C) Fluorescence images of PPT-PCR (upper: before magnetic separation; lower: after magnetic separation). (D) Gel electrophoresis image of PPT-PCR.

(Fig. 6A). The LOD was calculated from the linear detection ranges of the end-point fluorescence-based PPT-PCR (fluorescence = −2605 + 1891log [Lambda DNA] (R^2 = 0.98548)). The calculated LOD was 3.3 copies per μL ($3\sigma_{Blank}$). We confirmed that the magnetic separation and end-point fluorescence measurement processes could be completed within 15 seconds including 200 milliseconds of integration time (Fig. 6C). Therefore, the assay including 30 thermocycles and end-point fluorescence measurement can be completed in ~5.5 minutes. The analytical performance and LOD of PPT-PCR were compared with a conventional PCR thermocycler (Fig. 6B). Due to the system limitation, the cycling conditions of the conventional PCR instrument was adjusted to 95 °C, 20 seconds for initial denaturation; 95 °C, 5 seconds for denaturation; and 72 °C, 10 seconds for annealing and extension (the total time for 30 thermocycles was 30 minutes), because it cannot generate a reproducible amplification performance under ultrafast thermocycling conditions of PPT-PCR. The reaction mixtures without PMNs were tested with a conventional PCR thermocycler, fluorescence signals were measured after the PCR amplification and the calculated LOD was 6.8 copies per μL (Fig. 6B). The results indicated that PPT-PCR has similar levels of sensitivity and performance to commercial equipment, but with an approximately 5.5 times faster thermocycling time. The amplification products of PPT-PCR were further characterized by agarose gel electrophoresis and compared with the products from a conventional PCR thermocycler (Fig. 6D and S10). The clear changes in band intensities well matched with the changes in end-point fluorescence measurements and there was no significant difference between the two systems, indicating comparable performance.

Conclusions

In conclusion, we demonstrated a rapid and sensitive fluorescence biosensor based on plasmonic PCR using plasmonic magnetic nanoparticles for plasmonic photothermal heating as nano-sized heaters and fast fluorescence detection *via* magnetic separation. The shortest analysis time was achieved by optimizing LED intensity and the concentration of particles, demonstrating an ultrafast PPT-PCR that can complete 30 thermocycles and fluorescence detection in about 5.5 minutes. In the end-point fluorescence quantification of the amplified product, PPT-PCR shows a wide dynamic range, and the LOD achieved for the Lambda DNA template (3.3 copies per μL) is comparable to the sensitivity of conventional PCR equipment. Thus, compared to conventional real-time qPCR and other high-speed photonic PCR, our bi-functional nanoparticle and fluorescence detection-based PPT-PCR shows great advantages in both time- and cost-effectiveness and detection sensitivity (Table S1†). We believe that our strategy will be the basis for researchers to develop sensitive, inexpensive, highly mobile and low-energy methods that will allow researchers to quickly and accurately identify diseases through well-established NAA techniques.

Author contributions

Jingrui Wu: Methodology, investigation, formal analysis, software, writing the original draft. Kunlun Jiang: Methodology, investigation. Hua Mi: Methodology. Yuwei Qiu: Methodology. Jiwoong Son: Methodology, investigation. Hyun June Park: Investigation. Jwa-Min Nam: Investigation. Jung-Hoon Lee: Conceptualization, resources, writing, review and editing of the manuscript, supervision, funding acquisition. The manuscript was written through contributions from all authors. All authors have given approval to the final version of the manuscript.

Conflicts of interest

There are no conflicts to declare.

Acknowledgements

The authors acknowledge funding support from the City University of Hong Kong to J.-H.L (Project No. 9667180 and 7200583).

Notes and references

1 J. Liu, Z. Cao and Y. Lu, *Chem. Rev.*, 2009, **109**, 1948–1998.
2 N. J. Loman, C. Constantinidou, J. Z. M. Chan, M. Halachev, M. Sergeant, C. W. Penn, E. R. Robinson and M. J. Pallen, *Nat. Rev. Micro.*, 2012, **10**, 599–606.
3 I. G. Wilson, *Appl. Environ. Microbiol.*, 1997, **63**, 3741–3751.
4 A. K. Winter and S. T. Hegde, *Lancet Infect. Dis.*, 2020, **20**, 758–759.
5 Y. Wang, H. Kang, X. Liu and Z. Tong, *J. Med. Virol.*, 2020, **92**, 538–539.
6 C. J. Wang, C. Y. Ng and R. H. Brook, *J. Am. Med. Assoc.*, 2020, **323**, 1341–1342.
7 M. Salathé, C. L. Althaus, R. Neher, S. Stringhini, E. Hodcroft, J. Fellay, M. Zwahlen, G. Senti, M. Battegay and A. Wilder-Smith, *Swiss Med. Wkly.*, 2020, **150**, 1112.
8 T. Kilic, R. Weissleder and H. Lee, *Iscience*, 2020, 101406.
9 M. P. Cheng, J. Papenburg, M. Desjardins, S. Kanjilal, C. Quach, M. Libman, S. Dittrich and C. P. Yansouni, *Ann. Intern. Med.*, 2020, **172**, 726–734.
10 R. Weissleder, H. Lee, J. Ko and M. J. Pittet, *Sci. Transl. Med.*, 2020, **12**, eabc1931.
11 G. T. Walker, M. S. Fraiser, J. L. Schram, M. C. Little, J. G. Nadeau and D. P. Malinowski, *Nucleic Acids Res.*, 1992, **20**, 1691–1696.
12 M. C. Little, J. Andrews, R. Moore, S. Bustos, L. Jones, C. Embres, G. Durmowicz, J. Harris, D. Berger and K. Yanson, *Clin. Chem.*, 1999, **45**, 777–784.
13 M. Nilsson, H. Malmgren, M. Samiotaki, M. Kwiatkowski, B. P. Chowdhary and U. Landegren, *Science*, 1994, **265**, 2085–2088.
14 K. A. Heyries, C. Tropini, M. VanInsberghe, C. Doolin, I. Petriv, A. Singhal, K. Leung, C. B. Hughesman and C. L. Hansen, *Nat. Methods*, 2011, **8**, 649–651.
15 E. A. Ottesen, J. W. Hong, S. R. Quake and J. R. Leadbetter, *Science*, 2006, **314**, 1464–1467.
16 M. Baker, *Nat. Methods*, 2010, **7**, 351–356.
17 C. Zhang and D. Xing, *Nucleic Acids Res.*, 2007, **35**, 4223–4237.
18 F. Postollec, H. Falentin, S. Pavan, J. Combrisson and D. Sohier, *Food Microbiol.*, 2011, **28**, 848–861.
19 C. J. Smith and A. M. Osborn, *FEMS Microbiol. Ecol.*, 2009, **67**, 6–20.
20 R. Girones, M. A. Ferrus, J. L. Alonso, J. Rodriguez-Manzano, B. Calgua, A. de Abreu Corrêa, A. Hundesa, A. Carratala and S. Bofill-Mas, *Water Res.*, 2010, **44**, 4325–4339.
21 K. M. Horsman, J. M. Bienvenue, K. R. Blasier and J. P. Landers, *J. Forensic Sci.*, 2007, **52**, 784–799.
22 T. Yang, Z. Luo, Y. Tian, C. Qian and Y. Duan, *TrAC, Trends Anal. Chem.*, 2020, **124**, 115795.
23 S. L. Mitchell and K. S. George, *J. Clin. Virol.*, 2020, **128**, 104429.
24 G.-S. Park, K. Ku, S.-H. Baek, S.-J. Kim, S. I. Kim, B.-T. Kim and J.-S. Maeng, *J. Mol. Diagn.*, 2020, **22**, 729–735.
25 J. H. Son, B. Cho, S. Hong, S. H. Lee, O. Hoxha, A. J. Haack and L. P. Lee, *Light: Sci. Appl.*, 2015, **4**, e280–e280.
26 J. Kim, H. Kim, J. H. Park and S. Jon, *Nanotheranostics*, 2017, **1**, 178.
27 J. A. Webb and R. Bardhan, *Nanoscale*, 2014, **6**, 2502–2530.
28 S. Link and M. A. El-Sayed, *Int. Rev. Phys. Chem.*, 2000, **19**, 409–453.
29 J. R. Cole, N. A. Mirin, M. W. Knight, G. P. Goodrich and N. J. Halas, *J. Phys. Chem. C*, 2009, **113**, 12090–12094.

30 J.-H. Lee, M.-H. You, G.-H. Kim and J.-M. Nam, *Nano Lett.*, 2014, **14**, 6217–6225.
31 J. H. Lee, Z. Cheglakov, J. Yi, T. M. Cronin, K. J. Gibson, B. Tian and Y. Weizmann, *J. Am. Chem. Soc.*, 2017, **139**, 8054–8057.
32 M. You, Z. Li, S. Feng, B. Gao, C. Yao, J. Hu and F. Xu, *Trends Biotechnol.*, 2020, **38**, 637–649.
33 Y. Lee, B. H. Kang, M. Kang, D. R. Chung, G. S. Yi, L. P. Lee and K. H. Jeong, *ACS Appl. Mater. Interfaces*, 2020, **12**, 12533–12540.
34 B. Cho, S. H. Lee, J. Song, S. Bhattacharjee, J. Feng, S. Hong, M. Song, W. Kim, J. Lee, D. Bang, B. Wang, L. W. Riley and L. P. Lee, *ACS Nano*, 2019, **13**, 13866–13874.
35 T. Walsh, J. Lee and K. Park, *Analyst*, 2015, **140**, 1535–1542.
36 J. Cheong, H. Yu, C. Y. Lee, J.-u. Lee, H.-J. Choi, J.-H. Lee, H. Lee and J. Cheon, *Nat. Biomed. Eng.*, 2020, **4**, 1159–1167.
37 A. Dragan, R. Pavlovic, J. McGivney, J. Casas-Finet, E. Bishop, R. Strouse, M. Schenerman and C. Geddes, *J. Fluoresc.*, 2012, **22**, 1189–1199.
38 J. Liu, Z. Sun, Y. Deng, Y. Zou, C. Li, X. Guo, L. Xiong, Y. Gao, F. Li and D. Zhao, *Angew. Chem., Int. Ed.*, 2009, **48**, 5875–5879.
39 C. S. Levin, C. Hofmann, T. A. Ali, A. T. Kelly, E. Morosan, P. Nordlander, K. H. Whitmire and N. J. Halas, *ACS Nano*, 2009, **3**, 1379–1388.
40 J.-w. Kim, D. Seo, J.-u. Lee, K. M. Southard, Y. Lim, D. Kim, Z. J. Gartner, Y.-w. Jun and J. Cheon, *Nat. Protoc.*, 2017, **12**, 1871.
41 X. Huang and M. A. El-Sayed, *J. Adv. Res.*, 2010, **1**, 13–28.
42 C.-H. Chou, C.-D. Chen and C. R. C. Wang, *J. Phys. Chem. B*, 2005, **109**, 11135–11138.
43 P. K. Jain and M. A. El-Sayed, *Chem. Phys. Lett.*, 2010, **487**, 153–164.
44 N. S. Abadeer and C. J. Murphy, *J. Phys. Chem. C*, 2016, **120**, 4691–4716.
45 G. Schneider, G. Decher, N. Nerambourg, R. Praho, M. H. V. Werts and M. Blanchard-Desce, *Nano Lett.*, 2006, **6**, 530–536.